Deformation-phase measurement of diffuse objects that have started nonrepeatable dynamic deformation

Deformation-phase measurement of diffuse objects that have started nonrepeatable dynamic deformation

Masaaki Adachi, Jon N. Petzing, and David Kerr

We have developed what we believe is a new technique for obtaining a whole-field image representing the deforming amounts of a diffuse object. The object is supposedly continuously deforming and does not stop deforming during the measurement. This technique uses arccosine operations to extract the absolute, not signed, value of the phase. We assume that a right-phase change retains almost the same value in a small local area. This retention determines the sign of the phase and consequently the value of the phase change. The deformation phase during any term of the deforming process is shown as a map through the temporal-phase unwrapping of the calculated phase. © 2001 Optical Society of America

OCIS codes: 120.5050, 120.6160, 120.4290.

1. Introduction

The real-time deformation measurement of a diffuse object can be easily carried out with digital speckle pattern interferometry (DSPI). Because the phase change in the DSPI is quantitatively related to the amount of deformation, many studies have been done to extract accurate phase changes from specklegrams. For example, phase-shifting, specially designed multicamera, max–min scanning, Fourier-transform of carrier fringes, and spatial-carrier phase-shifting techniques have been reported.[1–6] Among them, the phase-shifting technique has been extensively investigated and applied to many practical measurements because of its simplicity and high resolution. It requires that several specklegrams be captured in the static, nondeforming, condition of a object, making it unsuitable for measuring objects deforming continuously. Even in conditions of continuous deformation, techniques that use the multicamera,[2] the Fourier transform,[5] and spatial-carrier phase shifting[6] can work well. However, they have individual disadvantageous points. The multicamera system is expensive. The Fourier-transforming[7] and spatial-carrier phase-shifting techniques[6] have considerably less resolution than the phase-shifting technique.[1] In the max–min scanning techniques,[3,4] two specklegrams are necessary to extract one speckle phase: one was of a deforming object and the other was of a sign image, phase-shifted to the former. Then they were applied to slowly deforming objects. Recently, some techniques that could extract a phase from only one specklegram of a deforming object[8,9] also have been proposed. To extract the phase, these techniques required the phase of the specklegram before deformation. Then they needed a static condition of the object in order to calculate the required phase through the phase-shifting technique.

The new technique proposed in this paper can be used to measure the deformation of objects that have already started a dynamic deformation and that keep deforming. During the measurement, specklegrams were continuously captured at a rate of 30 frame/s into the computer. Only in the initial stage of the capturing process was a reference optical path shortened at a certain rate. The specklegrams captured in this early stage were used to extract the phase at the starting point of the capturing process. From the light intensities of the specklegrams captured after the initial stage and the extracted phase, the technique extracted the speckle phase at their capturing moments without time-consuming calculations[8] of the histogram.

2. Phase Extraction

In Subsection 2.A we describe the extraction technique relating to the speckle phase at the starting

M. Adachi (adachi@t.kanazawa-u.ac.jp) is with the Department of Mechanical Systems Engineering, Faculty of Engineering, Kanazawa University, 2-40-20 Kodatsuno, Kanazawa 920-8667, Japan. J. N. Petzing and D. Kerr are with the Department of Mechanical Engineering, Loughborough University of Technology, Loughborough LE11 3TU, UK.

Received 19 March 2001; revised manuscript received 2 July 2001.

0003-6935/01/346187-06$15.00/0

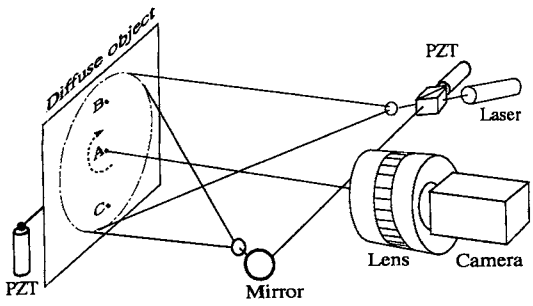

Fig. 1. Optical layout of a DSPI, which is also used in our experiment.

point of capturing process. Subsection 2.B concerns the technique to extract the changing phase after the starting point. The technique for obtaining the deformation phase during any term in the deformation process is described in Subsection 2.C.

A. Speckle Phase at the Starting Point of the Capturing Process

We consider the speckle interferometry shown in Fig. 1. The interference light intensity $I(\mathbf{r}, t)$ at time t and position $\mathbf{r}$ in a diffuse object is given by

$$I(\mathbf{r}, t) = O_D(\mathbf{r}) + O_{\mathrm{ALT}}(\mathbf{r})\cos\{\psi(\mathbf{r}, t)\}, \qquad (1)$$

where $O_D(\mathbf{r})$ is the dc component, $O_{\mathrm{ALT}}(\mathbf{r})$ is the modulation amplitude, and $\psi(\mathbf{r}, t)$ is the phase of the specklegram. When the object is continuously deforming a change in $I(\mathbf{r}, t)$ is shown by the curve in Fig. 2. Recording such an intensity change with a CCD camera gives the maximum and the minimum values, $I_{\max}(\mathbf{r})$ and $I_{\min}(\mathbf{r})$, of the light intensity change on an each pixel. From those values and light intensity $I(\mathbf{r}, t_k)$ in speckle image k, which is captured at $t = t_k$, the absolute value of the speckle phase $|\psi(\mathbf{r}, t_k)|$ can be calculated by

$$|\psi(\mathbf{r}, t_k)| = \cos^{-1}\left\{\frac{I(\mathbf{r}, t_k) - \left[\dfrac{I_{\max}(\mathbf{r}) + I_{\min}(\mathbf{r})}{2}\right]}{\left[\dfrac{I_{\max}(\mathbf{r}) - I_{\min}(\mathbf{r})}{2}\right]}\right\}. \qquad (2)$$

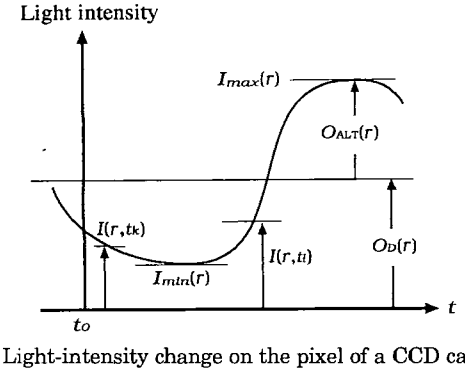

Fig. 2. Light-intensity change on the pixel of a CCD camera due to deformation of the object.

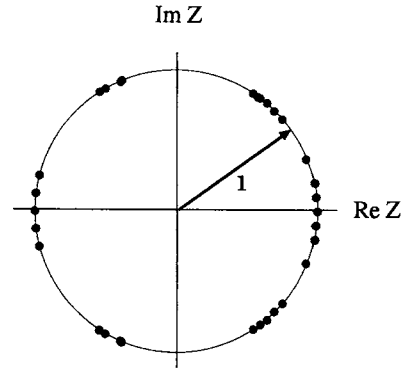

Fig. 3. Complex plane plotting of $\exp[i\delta_{kl}(\mathbf{r})]$ in a local area (3 × 3 pixels) where $\delta_{kl}(\mathbf{r})$ is given by Eq. (3). The number of points is 36 and some overlap.

We cannot determine a sign, plus or minus, because arccosine is an even function. One of the two values with opposite signs is a right phase and the other is not. Then we consider both signed phases and also consider a deformation phase from t_k to t_l. The following four values $\delta_{kl}(\mathbf{r})$ given by

$$\delta_{kl}(\mathbf{r}) = \pm|\psi(\mathbf{r}, t_l)| - \{\pm|\psi(\mathbf{r}, t_k)|\} \qquad (3)$$

are possible solutions for the deformation phase from t_k to t_l. Only one of the four values is right. Such right deformation phases on pixels in a small local area (for example, 3 × 3 pixels) around $\mathbf{r}$ should nearly equal one another, because amounts of deformation on pixels in such an area are supposed to be approximately the same. On a complex plane we plotted the value of $\exp[i\delta_{kl}(\mathbf{r})]$ in every pixel position in the small local area. Figure 3 shows the plotted points distributed symmetrically around the real axis. This symmetry comes from the fact that group values of $\delta_{kl}(\mathbf{r})$ in a small local area are the same as those of $-\delta_{kl}(\mathbf{r})$. Here we restrict our discussion of the distribution to only the upper half of the plane. In those areas 50% of the plotted points are related to the absolute values of the right deformation phases. The other points are affected by random speckle phases that originate from diffuse surface reflection.[8] They are statistically distributed uniformly from 0 to π in phase.

An average value of the points affected by the speckle phase was predicted to be close to $(2/\pi)i$. We therefore average all the plotted values in the upper half of the area and subtract $(2/\pi)i$ from the average value so that we can obtain the absolute value of the deformation phase. Although we have discussed the value of $\exp[i\delta_{kl}(\mathbf{r})]$, we actually average the values of $[I_{\max}(\mathbf{r}) - I_{\min}(\mathbf{r})]\exp[i\delta_{kl}(\mathbf{r})]$ instead of the values of $\exp[i\delta_{kl}(\mathbf{r})]$ so that low modulation data, which are sensitive to electric noise and digitizing error etc., can have less influence and high modulation data can have more influence on the average value. Figure 4 illustrates this. The curve in Fig. 2, which we introduced above in this section, is one of the recorded light-intensity changes. From those in-

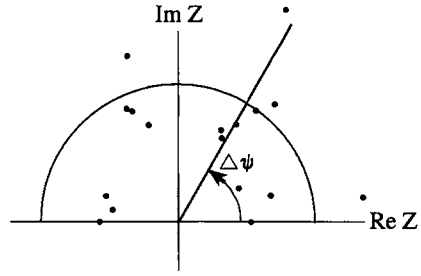

Fig. 4. Upper half complex plane plot of $Z = [I_{max}(\mathbf{r}) - I_{min}(\mathbf{r})]\exp[i\delta_{kl}(\mathbf{r})]$. $\Delta\psi$ is the phase of the average value for $[I_{max}(\mathbf{r}) - I_{min}(\mathbf{r})]\{\exp[i\delta_{kl}(\mathbf{r})] - (2/\pi)i\}$. The number of points is 18, and one point overlaps.

tensity changes the time dependence of the averaged value for $[I_{max}(\mathbf{r}) - I_{min}(\mathbf{r})]\{\exp[i\delta_{kl}(\mathbf{r})] - (2/\pi)i\}$ ($k = 0$, $l = 1, 2, 3, \ldots$) is calculated. Deformation phase $\Delta\psi$, derived from these averaged values, is also obtained and shown in Fig. 5. Deformation phase $\Delta\psi$ increases from $t = t_0$ to $t = t_m$ and reaches its maximum value around π at $t = t_m$. After $t = t_m$ it starts to decrease. This change can be explained: As the deformation gets larger, the points plotted in the upper half just after t_0 start to rotate more about the origin and move across the real axis into the lower half, while points in the lower half simultaneously move to the upper half. This fact implies that, if the deformation is less than π in phase, the absolute value of the deformation phase is correctly calculated.

Because only the absolute value of the deformation phase is obtained, the direction of the object deformation cannot be determined. In other words we do not know whether an optical path length increases or decreases. Therefore in the initial stage of the deformation measurement (the continuous capturing of specklegrams) we shorten the reference optical path length with a rate greater than the deformation speed. From the specklegrams captured during the shortening, the absolute deformation phase was calculated with the technique written above. The light-intensity changes at all the pixels during this shortening are related to the same direction in the

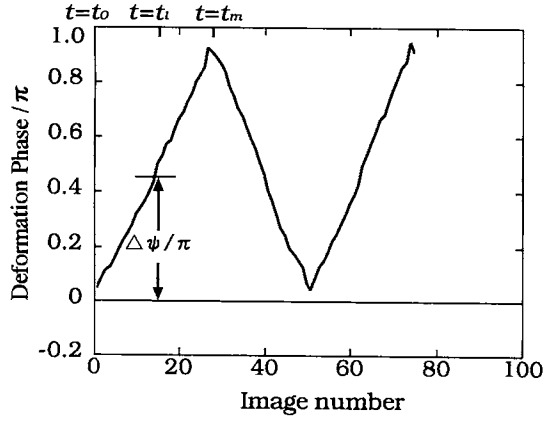

Fig. 5. Change in $\Delta\psi(\mathbf{r}, t)$ in Fig. 4 concerning the continuously deforming object.

phase change as that of only the shortening of the reference path length. Thus we can relate the phase change to the deformation direction correctly, which is positive under the shortening of the reference path length. Besides we can shorten the reference path length until the total phase changes during the shortening become greater than 2π on any pixel, so that we can obtain $I_{max}(\mathbf{r})$, $I_{min}(\mathbf{r})$ even at a nondeforming point.

In addition to $I_{max}(\mathbf{r})$ and $I_{min}(\mathbf{r})$ we already know $I(\mathbf{r}, t_0)$ (t_0 is the time of the starting point of the capture process) and $I(\mathbf{r}, t_j)$ (t_j is the time when the phase change due only to shortening becomes $\pi/2$ and the total phase change at t_j due to both shortening and deformation is bigger than 0 but less than π). From them $\cos[\psi(\mathbf{r}, t_0)]$ and $\cos[\psi(\mathbf{r}, t_j)]$ are easily calculated, and phase change $\Delta\psi(\mathbf{r}, t_j - t_0)[= \psi(\mathbf{r}, t_j) - \psi(\mathbf{r}, t_0)]$ is correctly extracted as shown in Fig. 5.

Regarding them, we can use

$$\cos[\psi(\mathbf{r}, t_0) + \Delta\psi(\mathbf{r}, t_j - t_0)] = \cos[\psi(\mathbf{r}, t_0)]\cos[\Delta\psi(\mathbf{r}, t_j - t_0)] - \sin[\psi(\mathbf{r}, t_0)] \times \sin[\Delta\psi(\mathbf{r}, t_j - t_0)]. \quad (4)$$

From Eq. (4) we can calculate $\sin[\psi(\mathbf{r}, t_0)]\sin[\Delta\psi(\mathbf{r}, t_j - t_0)]$ with

$$\begin{aligned}\sin[\psi(\mathbf{r}, t_0)]\sin[\Delta\psi(\mathbf{r}, t_j - t_0)] &= \cos[\psi(\mathbf{r}, t_0)]\cos[\Delta\psi(\mathbf{r}, t_j - t_0)] - \cos[\psi(\mathbf{r}, t_0) + \Delta\psi(\mathbf{r}, t_j - t_0)] \\ &= \cos[\psi(\mathbf{r}, t_0)]\cos[\Delta\psi(\mathbf{r}, t_j - t_0)] - \cos[\psi(\mathbf{r}, t_j)]. \end{aligned} \quad (5)$$

From $\sin[\psi(\mathbf{r}, t_0)]\sin[\Delta\psi(\mathbf{r}, t_j - t_0)]$ given by Eq. (5) and $\cos[\psi(\mathbf{r}, t_0)]\sin[\Delta\psi(\mathbf{r}, t_j - t_0)]$ obtained above, we can extract phase $\psi(\mathbf{r}, t_0)$ by

$$\psi(\mathbf{r}, t_0) = \arg\{\cos[\psi(\mathbf{r}, t_0)]\sin[\Delta\psi(\mathbf{r}, t_j - t_0)] + i\sin[\psi(\mathbf{r}, t_0)]\sin[\Delta\psi(\mathbf{r}, t_j - t_0)]\}. \quad (6)$$

Note that a change in phase $\psi(\mathbf{r}, t_0)$ is positive in shortening the reference path length. This phase can be extracted not only from the specklegram at t_j but also from all the specklegrams captured before t_j. Then $\cos[\psi(\mathbf{r}, t_0)]\sin[\Delta\psi(\mathbf{r}, t_k - t_0)] + i\sin[\psi(\mathbf{r}, t_0)]\sin[\Delta\psi(\mathbf{r}, t_k - t_0)]$ are calculated with k ($k < j$) and are plotted on the complex plane as shown in Fig. 6. By extracting the line intersecting the origin, O, and a gravity point of all the plotted points, $\psi(\mathbf{r}, t_0)$ can be extracted precisely.

B. Speckle Phase after the Starting Point of the Capturing Process

We calculate the absolute value $|\psi(\mathbf{r}, t)|$ of its speckle phase after the starting point in Eq. (2). Regarding the absolute value $|\psi(\mathbf{r}, t)|$ we also consider both signed values, $-|\psi(\mathbf{r}, t)|$ and $+|\psi(\mathbf{r}, t)|$, and calculate the phase change $\delta'(\mathbf{r}, t)$ from the starting point t_0 by

$$\delta'(\mathbf{r}, t) = \pm|\psi(\mathbf{r}, t)| - \psi(\mathbf{r}, t_0), \quad (7)$$

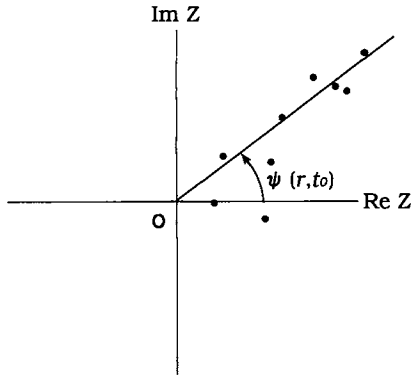

Fig. 6. Complex plane plotting of $\cos[\psi(\mathbf{r}, t_0)]\sin[\Delta\psi(\mathbf{r}, t_k - t_0)] + i \sin[\psi(\mathbf{r}, t_0)]\sin[\Delta\psi(\mathbf{r}, t_k - t_0)]$, where t_k is from t_0 to t_j.

where $\delta'(\mathbf{r}, t)$ has a right-phase change with a 50% possibility. For every pixel position in the local area around $\mathbf{r}$, we plot the values given by $[I_{\max}(\mathbf{r}) - I_{\min}(\mathbf{r})]\exp[i\delta'(\mathbf{r}, t)]$ on the complex plane. Figure 7(a) shows the plotted points, and we can see that the distribution of the plotted points has no symmetry. By averaging all the plotted points, we obtain a real component $C_r(\mathbf{r}, t)$ and an imaginary component $C_i(\mathbf{r}, t)$ of the average value. Deformation phase $\Delta\psi'(\mathbf{r}, t)$ after the starting point t_0 is then calculated as

$$\Delta\psi'(\mathbf{r}, t) = \arg[C_r(\mathbf{r}, t) + iC_i(\mathbf{r}, t)]. \quad (8)$$

As described above, one of the two values $\delta'(\mathbf{r}, t)$ in Eq. (7) is the right deformation phase, but the other is affected by a random speckle phase and is considered to be farther from $\Delta\psi'(\mathbf{r}, t)$ than the former. Therefore, concerning the two values, we eliminate the one that is farther from $\Delta\psi'(\mathbf{r}, t)$. Figure 7(b) shows the remaining values. The remaining values are almost related to the right deformation phase on the pixels in the local area, and $\Delta\psi''(\mathbf{r}, t)$ given by averaging over them is considered to be a more accurate deformation phase.

C. Deformation Phase during any Term

$\Delta\psi''(\mathbf{r}, t)$ is the wrapped value from $-\pi$ to π. Then we calculate an unwrapped value $\Delta\psi'''(\mathbf{r}, t)$ through temporally phase unwrapping by

$$\Delta\psi'''(\mathbf{r}, t_n) = \sum_{l=1}^{l=n} \arg\{\exp i[\Delta\psi''(\mathbf{r}, t_l) - \Delta\psi''(\mathbf{r}, t_{l-1})]\}. \quad (9)$$

The deformation phase during a term from t_p to t_q is given by

$$\phi(\mathbf{r}, t_q - t_p) = \Delta\psi'''(\mathbf{r}, t_q) - \Delta\psi'''(\mathbf{r}, t_p). \quad (10)$$

3. Experiment and Results

The optical layout used in this experiment is shown in Fig. 1. This layout confirms experimentally that the proposed technique can measure bidirectional dynamic deformation correctly. The beam from a laser diode, 50 mW in 780 nm, was divided by a beam splitter attached on a piezoelectric translator (PZT).

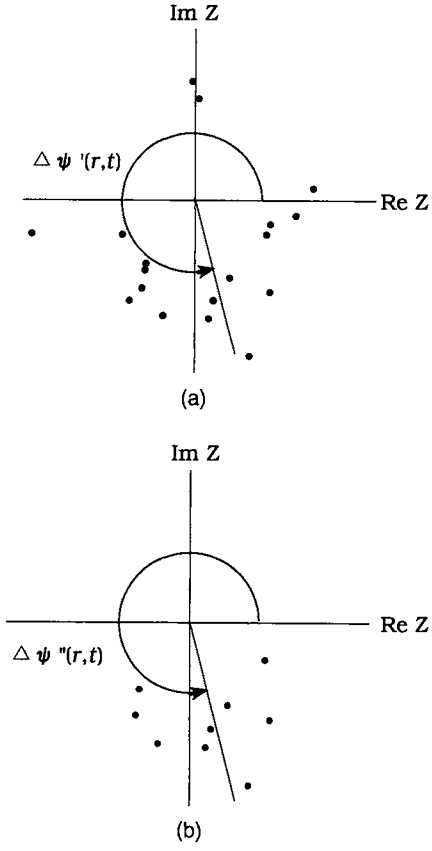

Fig. 7. (a) Complex plane plot of values calculated by $[I_{\max}(\mathbf{r}) - I_{\min}(\mathbf{r})]\exp[i\delta'(\mathbf{r}, t)]$. (b) Complex plane plot of the values that are selected from the points shown in Fig. 7(a).

The divided beams illuminated a diffuse object along the right oblique angle and the left oblique angle, respectively. Another PZT was set to rotate the diffuse object around the optical axis connecting point A in the object and the center of a CCD camera. When the object was rotated, an upper half side of the object and a lower half-side were deformed in opposite directions, and the amount of the deformation was shown by the rotated angle multiplied by the vertical component of the distance between a measured point and point A. Both PZTs were controlled by a computer. The CCD camera with 510 × 492 pixels was equipped with a zoom lens (Zoom NIKOR 35-105). Through the lens, a 25 mm × 25 mm area on the object was focused to 280 × 280 pixels in the CCD camera. A frame grabber board with an 8-bit analog-to-digital converter could capture the focused speckle image at a rate of 30 frame/s.

With the deformation measurement the diffuse object was rotated at a rate of ~0.1 mrad/s and specklegrams were continually captured. During only an initial 0.5 s from the start of the capturing process, the beam splitter attached to the PZT was also moved at a rate of ~1.5 μm/s.

Regarding the initial 10 frames of the captured specklegrams, $Z(\mathbf{r}, k) = \cos[\psi(\mathbf{r}, t_0)]\sin[\Delta\psi(\mathbf{r}, t_k - t_0)] + i \sin[\psi(\mathbf{r}, t_0)]\sin[\Delta\psi(\mathbf{r}, t_k - t_0)]$ were calculated at all the pixel positions of the object. Figure 6 shows

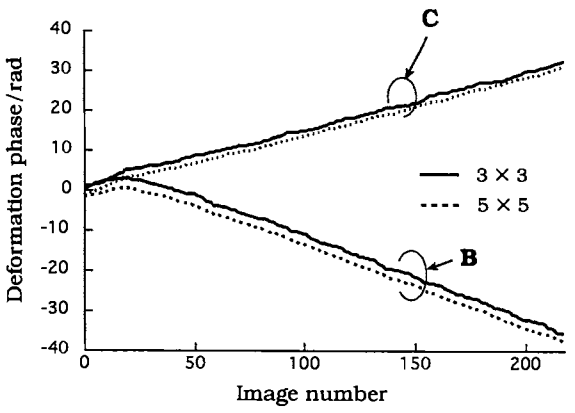

Fig. 8. Time dependencies of deformation phases about points B and C in Fig. 1: solid curves, dependence obtained by using a local area of 3 × 3 pixels; broken curves, that of 5 × 5 pixels.

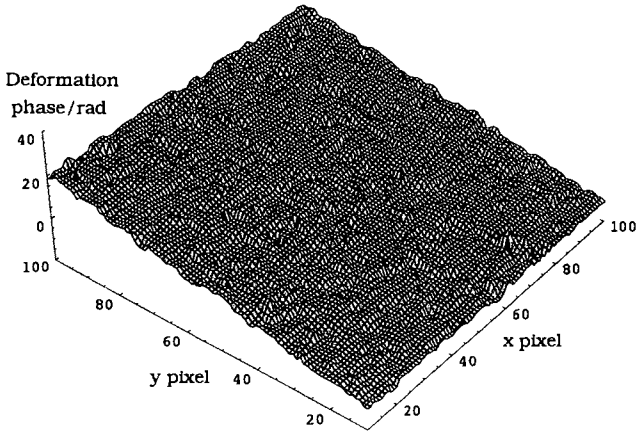

Fig. 10. Whole-field images of the deformation phase from the capturing start t_0 to t_{200}, where a local area of 3 × 3 pixels and a median filter of 3 × 3 pixels were used.

$Z(\mathbf{r}, k)$ plotted over $k(1 \le k \le 10)$ of a certain pixel. The plotted points were nearly distributed along the straight line intersecting the origin, O, meaning that the speckle phase $\psi(\mathbf{r}, t_0)$ calculated from each frames was nearly the same. This fact showed that the speckle phase $\psi(\mathbf{r}, t_0)$ was correctly measured.

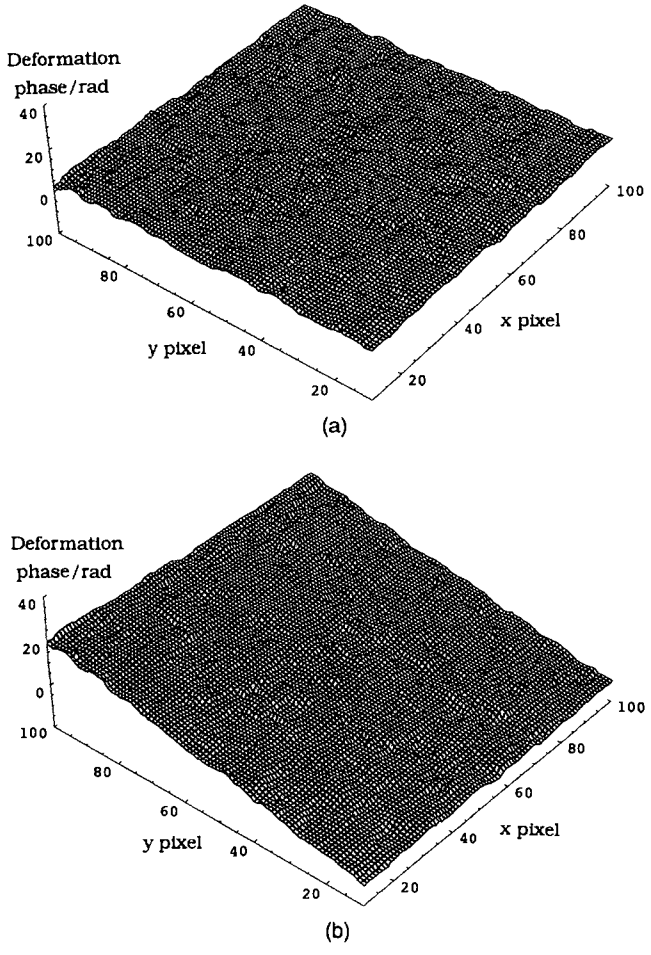

Fig. 9. Whole-field images of the deformation phase where a local area of 5 × 5 pixels and a median filter (5 × 5) were used. (a) From the capturing start t_0 to t_{20} (20th-frame capturing moment); (b) from the capturing start t_0 to t_{200}.

Nearly all the frames captured after t_0, $\Delta\psi'(\mathbf{r}, t)$, given by Eq. (8) were calculated. Then $\Delta\psi''(\mathbf{r}, t)$ was extracted by elimination of the values affected by a random speckle phase and by the averaging of the remained values. Finally $\Delta\psi'''(\mathbf{r}, t)$, and $\phi(\mathbf{r}, t - t_0)$ were obtained through Eqs. (9) and (10). Regarding points B and C of the diffuse object in Fig. 1, the time dependencies of $\phi(\mathbf{r}_B, t - t_0)$ and $\phi(\mathbf{r}_C, t - t_0)$ due to both PZT actions are shown in Fig. 8. In the first 15 frames $\phi(\mathbf{r}_C, t - t_0)$ increased faster than $\phi(\mathbf{r}_B, t - t_0)$. After that, $\phi(\mathbf{r}_C, t - t_0)$ still increased but at a lower rate. On the other hand, $\phi(\mathbf{r}_B, t - t_0)$ decreased. Both changing rates after the 15th frame were nearly constant, showing that deformation phases were measured correctly. In Fig. 8 the deformation phases were also shown when a local area size of 5 × 5 pixels was used. The whole-field image about the deformation phase from the capturing start t_0 to t_{20} (20th-frame capturing moment) is showed in Fig. 9(a) and that from t_0 to t_{200} is showed in Fig. 9(b). These images were obtained in the following condition: A local area of 5 × 5 pixels was used, and the phases calculated by Eq. (10) were then median (5 × 5) filtered. Figure 10 shows the whole-field image of the deformation phase from t_0 to t_{200}, which was obtained through both the local area of 3 × 3 pixels and a 3 × 3 median filter. The median filters were introduced easily to clear the difference between the processing of 5 × 5 pixels and 3 × 3 pixels.

The latter was somewhat worse in the signal-to-noise ratio. The above measured results show that the proposed technique can measure correctly the bidirectional dynamic deformation.

4. Discussions and Conclusions

In the images shown in Fig. 9 both the 5 × 5 pixel local area and the 5 × 5 pixel median filter were used. Figure 10 shows that the 3 × 3 pixel size of the local area and median filter considerably lowers the signal-to-noise ratio. Although a larger local size

lowers the lateral resolution of the deformation images, the proposed technique requires the lateral processing of a 5×5 pixel size to obtain a good signal-to-noise ratio. The main reason for these results is that the technique extracts the phase from only one specklegram in deformation, because a light-intensity change due to a phase change is given as a cosine function. The cosine function has a steep change area ($|d \cos \psi/d\psi| \fallingdotseq 1$), a less-steep change area ($|d \cos \psi/d\psi| \fallingdotseq 1/2$), and a nearly constant area ($|d \cos \psi/d\psi| \fallingdotseq 0$) with roughly the same possibility. At a certain moment in the deformation, light intensities on one third of the pixels might be in a nearly constant area.

In such conditions the phase calculated from the intensities would have to take a low signal-to-noise ratio. On the other hand, phase-shifting techniques use more than three specklegrams to extract one phase. At least one of the specklegrams would satisfy a steep-change condition in phase. Then it is inescapable that the technique extracting the phase from only one specklegram has a lower signal-to-noise ratio than the phase-shifting techniques. However, the proposed technique can extract the deformation phase of the object that has already started a dynamic deformation. The deformation phase of such an object cannot be extracted by normal phase-shifting techniques.

If we sacrifice a good signal-to-noise ratio to satisfy a high lateral resolution, the proposed technique can extract the deformation phase on only one pixel, not a laterally averaged phase. This high lateral resolution can be achieved through selecting one plotted point concerning the required pixel from the many points shown in Fig. 7(b). Although this selection would be affected by a continuity of the local deformation, the extracted phase was calculated from the light intensity recorded on the required pixel and would be a right phase with great possibility.

Phase noise due to speckle decorrelation also would affect the extracted phase. This effect degrades not only in the proposed technique but also in the phase-shifting technique and the like. Thus it is not considered here.

In conclusion, we have demonstrated that the proposed technique could correctly measure the deformation amount of the object that has already started nonrepeatable dynamic deformation. We believe that, if a technique is used with a high-speed and a high-lateral-resolution camera, a system can measure high-speed transient deformation with sufficient lateral and time resolutions.

This research was supported by a grant aid for General Scientific Research (C) (11650120) from the Ministry of Education, Science, Sports, and Culture of Japan.

References

1. K. Creath, "Phase-shifting speckle interferometry," Appl. Opt. **24,** 3053–3058 (1985).
2. A. J. P. Haasteven and H. J. Frankena, "Real-time displacement measurement using a multicamera phase-stepping speckle interferometry," Appl. Opt. **33,** 4137–4142 (1994).
3. E. Vikhagen, "Nondestructive testing by use of TV holography and deformation phase gradient calculation," Appl. Opt. **29,** 137–144 (1990).
4. J. Wang and I. Grant, "Electronic speckle interferometry, phase-mapping, and nondestructive testing techniques applied to real-time, thermal loading," Appl. Opt. **34,** 3620–3627 (1995).
5. A. Davila, D. Kerr, and G. H. Kaufmann, "Fast electro-optical system for pulsed ESPI carrier fringe generation," Opt. Commun. **123,** 457–464 (1996).
6. G. Pedrini and H. J. Tiziani, "Double-pulse electronic speckle interferometry for vibration analysis," Appl. Opt. **33,** 7857–7863 (1994).
7. M. Takeda, H. Ina, and S. Kobayashi, "Fourier-transform method of fringe-pattern analysis for computer-based topography and interferometry," J. Opt. Soc. Am. **72,** 156–160 (1982).
8. M. Adachi, Y. Ueyama, and K. Inabe, "Automatic deformation analysis in ESPI using one speckle interferometry of a deformed object," Opt. Rev. **4,** 429–432 (1997).
9. T. E. Carlsson and A. Wei, "Phase evaluation of speckle patterns during continuous deformation by use of phase-shifting speckle interferometry," Appl. Opt. **39,** 2628–2637 (2000).